1. Agenc

3. Report Type and Dates Covered.
Final - Journal Article

4. Title and Subtitle.
Forward scattering from fetch-limited and swell-contaminated sea surfaces

5. Funding Numbers.
Contract
Program Element No. 0601153N
Project No. 03202
Task No. 360
Accession No. DN257115
Work Unit No. 12212F

(2)

6. Author(s).
Jorge C. Novarini*, Richard S. Keiffer, and Jerald W. Caruthers

7. Performing Organization Name(s) and Address(es).
Naval Oceanographic and Atmospheric Research Laboratory
Ocean Acoustics and Technology Directorate
Stennis Space Center, MS 39529-5004

8. Performing Organization Report Number.
JA 221:024:92

9. Sponsoring/Monitoring Agency Name(s) and Address(es).
Naval Oceanographic and Atmospheric Research Laboratory
Basic Research and Management Office
Stennis Space Center, MS 39529-5004

10. Sponsoring/Monitoring Agency Report Number.
JA 221:024:92

11. Supplementary Notes.
*Planning Systems, Inc. 4455 Avenue A. Long Beach, MS 39560
Published in J. Acoust. Soc. Am.

12a. Distribution/Availability Statement.
Approved for public release; distribution is unlimited.

12b. Distribution Code

13. Abstract *(Maximum 200 words)*.

By using a Helmholtz-Kirchhoff (HK) approach described in a previous paper [J Acoust. Soc. Am. 91, 831-822(1992)], the forward scattering from nonfully developed sea surfaces is examined and the full three-dimensional scattering problem is addressed. Two types of departures from the limiting case of the fully developed sea are considered: fetch-limited seas and the more general case of seas that are time-evolving and swell-contaminated. Estimates of several statistical parameters of the forward scattered field are calculated for these surfaces as ensemble averages and are compared to those obtained for fully developed seas due to the same wind speed. Results are obtained for frequencies from 0.2 to 2 kHz, for moderate angles of incidence and moderate wind speeds. It is found that the fetch strongly affects the coherence and strength of the forward scattered field at and near the specular direction. In this frequency range, discrepancies in excess of 11 dB with respect to the fully developed case are predicted. For swell-contaminated surfaces, the scattering coefficient and the coherence are strongly influenced by the relative contributions of sea and swell to the total roughness and directional characteristics of the surface. Swell-contaminated sea surfaces having the same total roughness but different sea-swell compositions are shown to result in significantly different scattering patterns.

14. Subject Terms.
Acoustic scattering, reverberation, surface roughness

15. Number of Pages.
10

16. Price Code.

17. Security Classification of Report.	18. Security Classification of This Page.	19. Security Classification of Abstract.	20. Limitation of Abstract.
Unclassified	Unclassified	Unclassified	SAR

Forward scattering from fetch-limited and swell-contaminated sea surfaces

Jorge C. Novarini
Planning Systems, Inc., 4455 Avenue A, Long Beach, Mississippi 39560

Richard S. Keiffer and Jerald W. Caruthers
Naval Ocean Research and Development Activity, Stennis Space Center, Mississippi 39529-5004

(Received 11 December 1991; accepted for publication 27 May 1992)

By using a Helmholtz–Kirchhoff (HK) approach described in a previous paper [J. Acoust. Soc. Am. **91**, 831–822 (1992)], the forward scattering from nonfully developed sea surfaces is examined and the full three-dimensional scattering problem is addressed. Two types of departures from the limiting case of the fully developed sea are considered: fetch-limited seas and the more general case of seas that are time-evolving and swell-contaminated. Estimates of several statistical parameters of the forward scattered field are calculated for these surfaces as ensemble averages and are compared to those obtained for fully developed seas due to the same wind speed. Results are obtained for frequencies from 0.2 to 2 kHz, for moderate angles of incidence and moderate wind speeds. It is found that the fetch strongly affects the coherence and strength of the forward scattered field at and near the specular direction. In this frequency range, discrepancies in excess of 11 dB with respect to the fully developed case are predicted. For swell-contaminated surfaces, the scattering coefficient and the coherence are strongly influenced by the relative contributions of sea and swell to the total roughness and directional characteristics of the surface. Swell-contaminated sea surfaces having the same total roughness but different sea-swell compositions are shown to result in significantly different scattering patterns.

PACS numbers: 43.30.Hw, 43.20.Fn

INTRODUCTION

A review of the literature to date reveals that, in general, theoretical and numerical studies of underwater acoustic scattering from the air/sea interface have restricted themselves to sea surfaces that are fully developed. In addition, modeling efforts are often simplified by assuming that the seas are one dimensional (1D or "long-crested") or isotropic. In part, this has been due to a lack of adequate and readily available characterizations for the more complex seas that result from spatially nonuniform and temporally nonstationary generating winds. On the other hand, the 3-D nature of acoustic scattering from two-dimensional (2-D) fully developed sea surfaces has not yet been adequately explored.

Implicit in the description of a fully developed sea surface is the assumption that the time duration of the constant generating winds as well as the spatial extent over which the wind is acting (the fetch) are very large. In reality, for a given wind speed, it can take several hours of constant wind acting over the sea for several tens of kilometers to produce a surface that approaches the limiting case of the fully developed sea. In coastal regions and for high enough wind speeds, the seas will never reach the fully developed state due to the limited fetch conditions. Also, the wind field generating the sea surface is typically not uniform over large areas and frequently swell due to distant or previous weather activity can contaminate the local seas.

Spectral descriptions of wind-driven sea surfaces that take into account the effects of the fetch have been available for some time but have been relatively unexplored by the acoustics community. More recently, second generation spectral models have become available that produce the numerical 2-D spectrum of the sea from the time evolution of the wind field specified over a wide area. This allows for the calculation of the acoustic scattering from seas that are generated by nonuniform, nonstationary wind fields. As an example, spectral models of this kind can be used to consider the impact of swell from distant weather conditions on the acoustic scattering. The aim of the present work is to first analyze, as a prelude to more complex surfaces, the forward scattering from 2-D sea surfaces generated by wind fields that are spatially uniform, stationary in time but are under fetch-limited conditions and then to extend this analysis to sea surfaces that are produced by nonstationary, nonuniform wind fields and contaminated by swell. The full three-dimensional nature of the forward scattering problem will be addressed. To accomplish these objectives, a modeling technique[1] is employed which essentially consists of simulating a sea surface (or surfaces) having a particular surface height probability density function (PDF) and 2-D power spectrum of surface elevations and calculating the complex scattered pressure field at the receiver by numerically integrating the Helmholtz–Kirchhoff (HK) kernel over each

surface realization. The moments of the scattered field are then obtained as ensemble averages. This technique has become quite popular in the acoustics literature and is often called "Monte Carlo." Since the effects of shadowing and multiple scattering are ignored in this approach, and due to the inherent limitations imposed by the Kirchhoff approximation,[2] the analysis is restricted to moderate grazing angles and the forward scatter direction.

This paper is organized as follows. In the first section, the modeling approach is briefly reviewed. The second section considers the acoustic results from sea surfaces generated under uniform, stationary, but fetch-limited conditions. In the third section, results due to sea surfaces generated by nonstationary, nonuniform wind fields are considered. In particular, this latter section begins to assess the effects of the swell on the forward scattered acoustic field. In all cases, results will be compared with those from fully developed sea surfaces in order to get an estimate of the discrepancies that may arise when one naively assumes a fully developed sea.

I. MODELING APPROACH

A. Modeling ocean surfaces

Randomly rough surfaces having a particular power spectrum and surface height PDF may be generated in a number of ways. We have adopted a 2-D linear filter technique that has been described elsewhere.[1,3] Multiple realizations of a particular spectral type were achieved by making the output surface large enough for 30 statistically independent scattering patches to fit on it. In this study, the input surface was chosen to have a Gaussian PDF of surface heights. The fidelity of the numerical surfaces was determined through a comparison of their autocovariance functions (ACF) with the Fourier transformation of the corresponding theoretical surface spectra.

Three types of spectra have been adopted for this work. They are: the Pierson–Moskowitz (PM) spectrum[4] to characterize fully developed surfaces, the JONSWAP spectrum[5] for surfaces generated by temporally stationary, spatially uniform, but fetch-limited wind fields, and the global/regional deep water wave model[7] (DWAVE) for surfaces generated by nonstationary, nonuniform wind fields. Unlike the Pierson–Moskowitz or JONSWAP descriptions, DWAVE numerically calculates the directional wave spectrum at a given location based on the time-evolving wind fields and other environmental information in the surrounding region. Thus swell components generated by distant storms or by previous winds are incorporated in the spectral description. Note that while in the acoustic literature the term "swell" is sometimes used to refer to the low-frequency components of a wind-driven wave system, in this work we adopt the oceanographic terminology[7] and define "sea" as the spectral components of the surface driven by the local wind, and swell as the low-frequency components not induced by the local wind. Therefore, the swell does not necessarily have the same direction as the sea.

The Pierson–Moskowitz spectrum has been used extensively in the scattering literature. Assuming a cosine-squared directional dependence,[8] the spectral density is given by

$$S_{\mathrm{PM}}(f,\theta)=\frac{\alpha}{8\pi^5}\frac{g^2}{f^5}\exp\left[-\frac{5}{4}\left(\frac{f_{\max}}{f}\right)^4\right]\cos^2\theta, \tag{1}$$

where α is the so-called Philips constant ($\alpha=0.0081$), g is the acceleration due to gravity, θ is the wave direction with respect to the wind direction, f is the wave frequency in Hz, and $f_{\max}=0.14\,g/U$ (U is the wind speed measured 19.5 m above sea level) is the wave frequency at which the spectrum peaks.

Very similar in form (and again assuming a cosine-squared directional dependence) but with certain additional fetch-dependent parameters is the JONSWAP spectrum:

$$S_{\mathrm{JW}}(f,\theta)=\frac{\alpha^*}{8\pi^5}\frac{g^2}{f^5}\exp\left[-\frac{5}{4}\left(\frac{f^*_{\max}}{f}\right)^4\right]\gamma^q\cos^2\theta, \tag{2}$$

where

$$q=\exp\left(-\frac{(f-f^*_{\max})^2}{2\sigma^2(f^*_{\max})^2}\right) \tag{3}$$

and

$$\sigma=\begin{cases}0.07, & f\leqslant f^*_{\max},\\ 0.09, & f\geqslant f^*_{\max}.\end{cases} \tag{4}$$

The constant α^*, as well as the peak frequency $f^*_{\max}$, are now fetch-dependent parameters. Defining the normalized fetch z in terms of wind speed and the fetch (x):

$$z=gx/U^2, \tag{5}$$

these parameters are given by

$$\alpha^*=0.074/z^{0.22}, \tag{6}$$

and

$$f^*_{\max}=3.57g/Uz^{0.33}. \tag{7}$$

These equations have been modified for U measured at 19.5 m above sea level (the original JONSWAP equations refer to the wind measured 10 m above sea level) to facilitate comparisons with results from surfaces having a Pierson–Moskowitz spectrum. The parameter γ is the so-called peak enhancement factor which is only weakly fetch dependent. Hasselman[5] *et al.* have proposed that a constant value for γ be adopted ($\gamma=3.3$). Finally, it should be mentioned here that, in the open ocean, where it is difficult to define the fetch, the peak frequency of the observed spectrum can be used to define an "effective" fetch through Eq. (7).

The transition to a fully developed sea occurs in the very final stages of surface development and Eq. (2) does not attempt to describe such seas. As a consequence, in the present work, the transition stage will be avoided. To that end, it is necessary to estimate the fetch at which the crossover between the two regimes occurs. In this work, the crossover fetch is taken to be the fetch at which the peak frequency of the fetch-limited sea, given by Eq. (7) equals the peak frequency of a fully developed sea. The resulting crossover fetch for a given wind speed (m/s) is then

$$x_{\mathrm{crossover}}=1.86U^2\ (\mathrm{km}). \tag{8}$$

The effect that the fetch has on the surface spectrum can be seen clearly in Fig. 1. Shown here are spectral profiles in the up/downwind direction for a wind speed of 11 m/s and several values of fetch. Note the striking differences in spec-

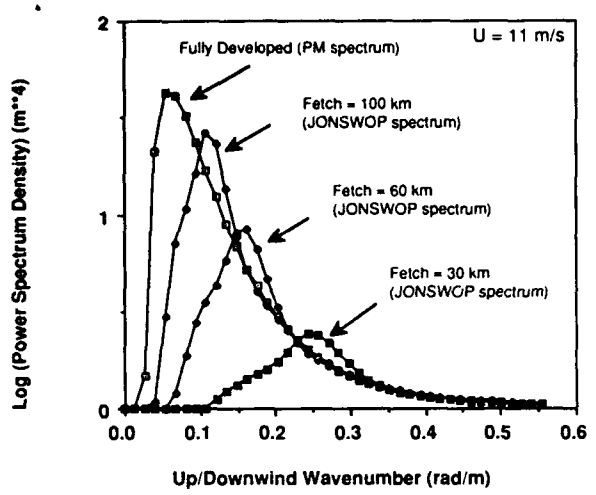

FIG. 1. Power spectra in the up/downwind direction for fully developed and fetch-limited seas driven by an 11-m/s wind.

tral shape and energy content between the fully developed sea and the fetch-limited seas. In general, the shorter the fetch the higher the peak wave number and the smaller the amplitude or roughness associated with the spectral peak.

In order to allow direct comparisons among the acoustic fields scattered from different sea surfaces, common windward and crosswind grid spacings ($\Delta x = 1.36$ and $\Delta y = 2.85$ m, respectively) were adopted for all surfaces considered. Since the maximum wave number is proportional to the inverse of the grid spacing, a common maximum wave number for all wind speeds is implied. Due to computational constraints on memory size and time, the surface spectrum was truncated at high frequencies excluding high-frequency gravity waves and capillary waves. In each case, energy in wavelengths shorter than 2.72 m in the x direction and shorter than 5.44 m in the y direction were excluded from the surface realizations. For each wind speed considered, the spectral resolutions (or minimum wave numbers in the up/downwind and crosswind directions), Δk_x and Δk_y, were determined to accommodate the longest significant wavelength included in the wavetrain. The number of spectral samples in the k_x and k_y direction (M and N, respectively) was then calculated through the relationships

$$M = \frac{\pi}{\Delta x\, \Delta k_x}; \quad N = \frac{\pi}{\Delta y\, \Delta k_y}. \tag{9}$$

For all of the 8-m/s surfaces, M and N were chosen to be 84 and 56, respectively. For the 11-m/s surfaces and the hybrid or swell-contaminated surfaces, which must be larger to accommodate the increase in low-frequency spectral information, M and N were chosen to be 170 and 108, respectively.

B. Acoustic scattering calculations

As mentioned earlier, the HK approach has been adopted in this work as a tool suitable for the analysis of the forward scattered field from Pierson–Moskowitz seas.[9] Since the HK integral is evaluated numerically, the complex scattered pressure from a 2-D surface is readily obtained. Assuming that the source and receiver be located further than a few wavelengths from the scattering surface, the following form for the HK integral is adopted:

$$P_s(\mathbf{r}) = \frac{ik}{4\pi} \int_s D(x',y') \frac{e^{ik(R_1 + R_2)}}{R_1 \cdot R_2} \left(\frac{\mathbf{R}_1}{R_1} - \frac{\mathbf{R}_2}{R_2} \right) \cdot \mathbf{n}\, ds', \tag{10}$$

where

$$\mathbf{R}_1 = \mathbf{r}' - \mathbf{r}_{\text{source}},$$
$$\mathbf{R}_2 = \mathbf{r}_{\text{receiver}} - \mathbf{r}', \tag{11}$$

and the integration indicated is over the scattering surface. Here, $D(x',y')$ is a Gaussian insonification function that has been added in the usual manner to minimize the contribution of the edges of the insonified region to the scattered field. Although this function is designed to fall 39 dB at the edges of the insonified surface, since each surface realization spans several correlation lengths (usually six or more depending upon the modeled surface), an area located at the center of the surface and measuring at least one correlation length on a side is uniformly insonified to within 1 dB. Note that no phase or slope approximations have been made to the HK kernel.

As described in the previous section, certain statistics of the scattered field are calculated as ensemble averages over many surface realizations. Of particular interest here are three parameters: the total and incoherent scattering coefficients (ρ and ρ_{inc}), the coherence (Γ). The second moment of the scattered field, or total intensity, $\langle P_s P_s^* \rangle$, can be decomposed[9] into a coherent component, $\langle P_s \rangle \langle P_s^* \rangle$, and an incoherent component or variance, v^2:

$$\langle P_s P_s^* \rangle = \langle P_s \rangle \langle P_s^* \rangle + v^2. \tag{12}$$

The total and incoherent scattering coefficients are defined by

$$\rho = \langle P_s P_s^* \rangle / P_0 P_0^*, \tag{13}$$

and

$$\rho_{\text{incoh}} = v^2 / P_0 P_0^*. \tag{14}$$

Here, P_0 is the specularly scattered pressure from an acoustically soft, flat surface under the same ensonification conditions.

We define the coherence for narrow-band signals as

$$\Gamma = \left(\frac{\langle P_s P_0^* \rangle^2}{\langle P_s P_s^* \rangle P_0 P_0^*} \right)^{1/2}. \tag{15}$$

The calculation of the statistical parameters of the scattered acoustic field begins with the creation of a large surface realization from which 30 statistically independent subareas are extracted and identically ensonified. The statistical moments of the complex scattered acoustic field were estimated as ensemble averages over these surfaces. A more complete description of the modeling technique is given in Ref. 1.

The results discussed here are expected to be accurate in the frequency range 0.2–2.0 kHz. The lower limit in this range is imposed by criteria for the validity of the Kirchhoff approximation, the upper frequency limit is imposed primarily by constraints on computational costs.

In addition to the limitations imposed by the Kirchhoff approximation, the results presented here also avoid low grazing angle scattering geometries so that the effects of shadowing can be safely ignored. Unless specified otherwise, the zenithal and azimuthal angles for the source and receiver are

$$\theta_{\text{source}} = \theta_{\text{receiver}} = 45°,$$
$$\phi_{\text{source}} = 180°, \qquad (16)$$
$$\phi_{\text{receiver}} = 0°.$$

The wind direction for the fetch-limited and fully developed sea surfaces is in the direction of the positive x axis ($\phi = 0$). The distances of the source and receiver to the center of the scattering area are also kept constant at 3500 m.

II. SCATTERING FROM FETCH-LIMITED SEA SURFACES

A. Specular scattering

In an earlier study, the influence of the fetch on forward scattering from the sea surface was studied by McDaniel and McCammon.[11] In that study, a composite roughness model was used to calculate the scattered field from seas characterized by the JONSWAP fetch-limited spectrum. It was further assumed in this study that the surfaces roughness was isotropic. Results from that study indicate that in the specular direction, for relatively high frequencies, the scattering strength from fetch-limited surfaces may be up to 10 dB higher than the strength from a fully developed sea generated by the same wind speed.

The influence of the fetch on the specularly scattered field will now be examined. Table I summarizes the effect of the fetch on the variance of the sea surface heights and on the spectral peak for two different wind speeds as compared to the fully developed sea having the same wind speed. Also given for each wind speed is the crossover fetch as calculated from Eq. (8). Since the transition region with a fully developed sea is to be avoided, the lower the wind speed the lower the maximum fetch considered. Thus, for an 8-m/s wind, fetches of 30 and 60 km are considered, and for an 11-m/s wind three fetches (30, 60, and 100 km) are considered. For both wind speeds, the largest fetch considered is approximately one-half of the crossover fetch for that wind speed as calculated from Eq. (8).

For a constant wind speed of 8 m/s, the influence of the fetch on the scattering coefficient and the coherence are shown in Fig. 2. Clearly, the effect of the fetch at this wind speed on the scattering coefficient and coherence can be quite appreciable. As expected of specular scattering at low frequencies, the two surfaces that have nearly the same total variance (the 60-km fetch and the fully developed surfaces in this case) have nearly the same frequency dependence. This appears to hold for the scattering coefficient up to about 1.6 kHz where, for the fully developed sea, the transition from a rough to a very rough surface occurs (i.e., total inten-

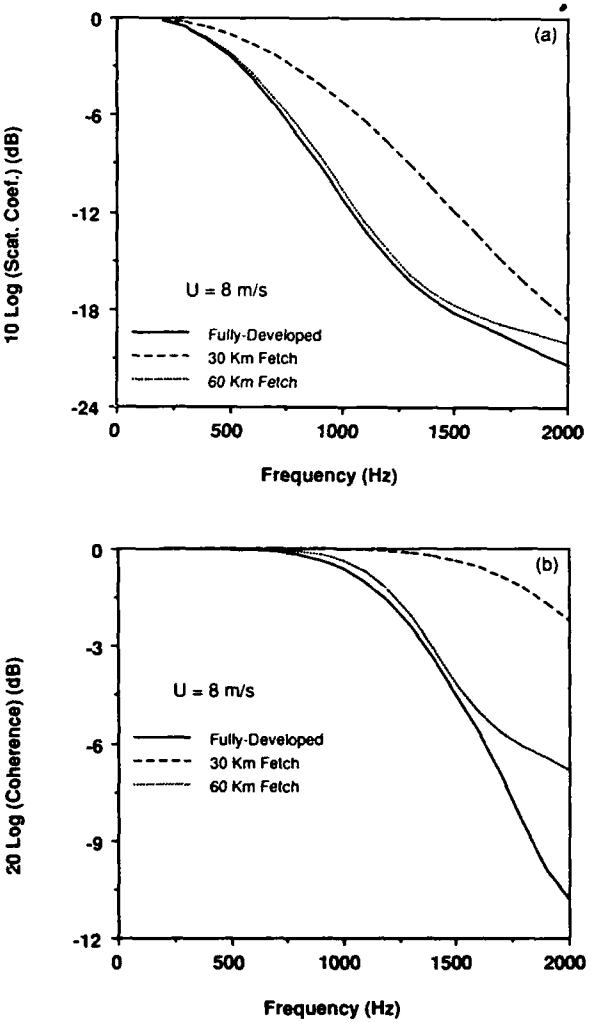

FIG. 2. The effect of the fetch in the specular direction on (a) scattering coefficient and (b) coherence. Wind speed is 8 m/s.

TABLE I. Characteristics of the fetch-limited surfaces. PM stands for Pierson–Moskowitz.

	Wind speed (m/s)						
	8			11			
Fetch (km)	30	60	PM	30	60	100	PM
σ^2 (m^2)	0.04	0.09	0.11	0.07	0.15	0.27	0.45
Λ_{peak} (m)	18	32	40	25	39	54	83
$X_{\text{crossover}}$ (km)		120			225		

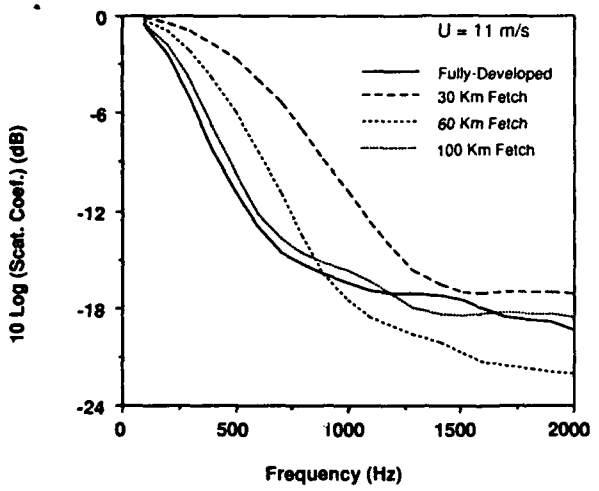

FIG. 3. The effect of the fetch in the specular direction on the scattering coefficient. Wind speed is 11 m/s.

sity–coherent intensity = 10 dB). It can be noted that at this frequency the coherence for the fully developed sea is approximately 6 dB down. The 30-km fetch surface, which has the rms roughness (but not the spectral content) of a much lower wind speed fully developed sea, results in much less loss and a much higher coherence. For example, at 1.5 kHz the scattering coefficient for the 30-km fetch case differs from the prediction for the fully developed surface by approximately 7.5 dB.

In Fig. 3, results for an 11-m/s wind speed show essentially the same effects. That is, the shorter the fetch the smoother the surface and therefore the stronger and more coherent the low-frequency specular scattering. At this higher wind speed, however, it is even more clear that the fetch can dramatically affect the scattering at all frequencies. At 700 Hz, for example, the scattering coefficient for the 100-km fetch case is approximately 10 dB lower than that predicted for the 30-km fetch case. As in the previous example, it is observed that the initial rolloffs for both parameters are determined by the rms roughnesses. However, for this higher wind speed, it can be observed that there are frequency bands over which a shorter fetch surface has a smaller scattering coefficient or coherence than one or several of the longer fetch cases. For example, at 900 Hz, the scattering coefficient for the 60-km case dips below both the 100-km and fully developed cases and stays lower out to the highest frequency considered. Similar curve crossings are also apparent in the plot of the coherence.

From these numerical experiments it can be concluded that in the specular direction, the fetch affects the coherence as well as the scattering coefficient at all wind speeds. The shorter the fetch, the higher the frequency at which the coherence first begins to degrade. The scattering coefficient is affected at all frequencies with deviations up to 11 dB. Note that similar discrepancies were reported by McCammon and McDaniel.[11] We might further speculate from this limited data set that whenever the fetch exceeds about half of the crossover fetch for any particular wind speed, differences in the scattering in the specular direction between the fetch-limited and fully developed seas are typically small.

Nonspecular forward scattering

To investigate the effect of the fetch on the scattered field in the vicinity of the specular direction, the receiver's position was allowed to vary ± 15 deg in and out of the plane of incidence while the source was held fixed ($\phi_s = 180°$, $\theta_s = 45°$). This analysis was carried out for the 11-m/s fully developed and 30-km fetch cases.

Figure 4 shows the effect (at 300 Hz) of the fetch on the total and incoherent scattering coefficients as a function of the receiver's zenith and azimuth, respectively. As expected, the 30-km fetch surface, which is considerably smoother, results in much less scattering out of the specular direction. Note that for the total scattering coefficient, the azimuthal variation results in a broader pattern than does the zenithal variation. For either variation, discrepancies in the total scattered energy between the fully developed and fetch-limited sea are in excess of 15 dB at angles just outside of the

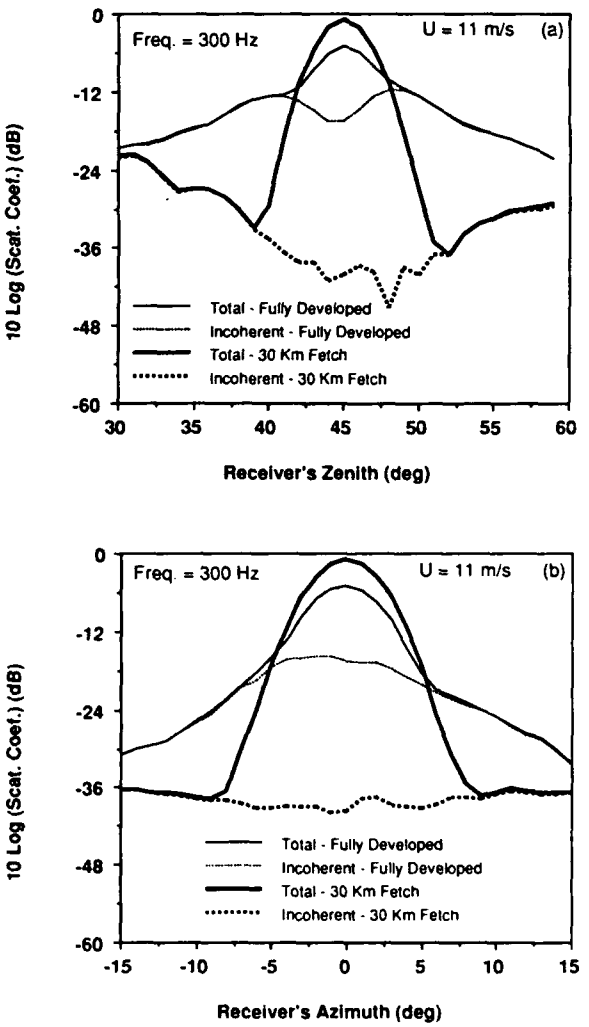

FIG. 4. The effect of the fetch on the total and incoherent scattering coefficients for scattering out of the specular direction: (a) zenithal variation and (b) azimuthal variation. Wind speed is 11 m/s; frequency = 300 Hz.

main beam of the fetch-limited case. As a final observation, it should be pointed out that, given the assumption of a $\cos^2 \phi$ dependence of the spectrum on azimuthal variation, it is expected that the plots of the scattering parameters should be symmetric with respect to variation of the receiver's azimuthal angle about the specular direction. It is evident from Fig. 4 that there is some departure from this symmetry particularly for the rougher fully developed surface. This is attributed to the fact that there are a limited number of realizations used to calculate the ensemble average. While the details in the differences between the two cases shown here and elsewhere in this paper are affected by this error, the conclusions reached, which are based on gross effects, are not.

Concerning the incoherent scattering coefficient, it is noted that in a first-order approximation, the incoherent scattering out of the specular direction is a Bragg-type resonance phenomenon.[12] Since the high-frequency spectral content of the fully developed surface is identical to that of the fetch-limited surface except for the narrow region of the spectral overshoot, the incoherent scattering coefficient is expected to be nearly the same for a fully developed surface as for a fetch-limited surface for the higher acoustic frequencies of interest in this study. On the other hand, the fetch-limited surfaces do not have the long surface waves present, and, therefore, at low frequencies the incoherent component is expected to show resonances for the fully developed sea that are not present for the 30-km fetch-limited case.

In Fig. 4(a), two Bragg resonances are evident for the fully developed surface. The incoherent scattering coefficient peaks at zenithal angles of approximately 40 and 50 deg for the fully developed surface, while at these angles there is little incoherent energy for the 30-km fetch case. This distinct behavior of the fetch-limited sea as compared with the fully developed sea can be interpreted in terms of resonant interaction with the dominant wavetrain. Assuming that the dominant wavelength of the spectrum is responsible for the resonant scattering patterns observed, it is easy to get from first-order perturbation theory the zenithal angles for Bragg scattering by the peak spectral component ($\lambda = 100$ m) of the fully developed surface. At an acoustic frequency of 300 Hz, this approach gives the same angles (40 and 50 deg) for the locations of the resonances. This long surface wavelength is very weak for the 30-km fetch case and, consequently, no resonances are observed at those angles. For the 30-km fetch case, however, the dominant wavelength, which is the region of spectral overshoot, is about 24 m. Consequently, at an acoustic frequency of approximately 1100 Hz (not shown), the fetch-limited surface should exhibit slightly enhanced resonances at zenithal angles of 40 and 50 deg as compared to the fully developed surface.

III. SCATTERING FROM SURFACES GENERATED BY NONSTATIONARY, NONUNIFORM WIND FIELDS

A. Swell-contaminated sea surfaces

The previous sections dealt with surfaces driven by the local wind alone. In reality, the sea surface is influenced by nearby as well as distant forcing phenomena, evolving over time in a complex manner. In order to examine acoustic scattering from sea surfaces that are nonstationary in time and due to nonuniform generating winds, the DWAVE model has been employed. This model numerically calculates the directional wave spectrum at a given geographical location based on the time-varying wind field and other environmental information specified over an extended region. This 2-D numerical spectrum is then used in the filtering process that has been described earlier in order to generate ensembles of scattering surfaces.

Since we are particularly interested in ocean surfaces having varying degrees of swell present, wind field data gathered after the passage of a storm are the most appropriate input data for the DWAVE model. To this end, historical wind records gathered off the Louisiana and Mississippi Gulf coast were used in the DWAVE model to generate four sea surface spectra (every 2 h over a 6-h period) at a location 60 km off the Louisiana coast (90 30′ W; 28 30′ N) starting approximately 6 h after hurricane Camille hit shore. Obviously, it is not the intention of this paper to model scattering from the surface at the time of the hurricane. At the time of these spectra, the local winds were quite moderate and decreasing in time. Furthermore, while Hurricane Camille cannot be considered a typical storm, sea conditions some time after the storm passes are representative of the time varying conditions that may be encountered at sea after more typical storms.

Shown in Fig. 5 is a comparison of the measured significant wave height versus time at a nearby location and the results from the DWAVE model for that location. Note that except for some time shifting of the events, the agreement is quite good. Shown in Fig. 6 are normalized contour plots of the directional surface spectra generated by the DWAVE model for the 6-h period of interest (henceforth referred to as cases or swell-contaminated surfaces A, B, C, D, respectively). The complex bimodal structures evidenced in these spectra are characteristic of directional sea surfaces that contain swell. It is clear from these plots that, though narrow, the swell is far from being a monochromatic component.

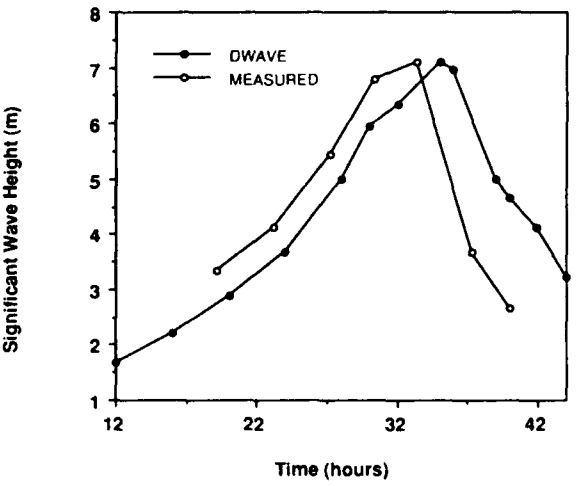

FIG. 5. Measured significant waveheight versus the DWAVE model

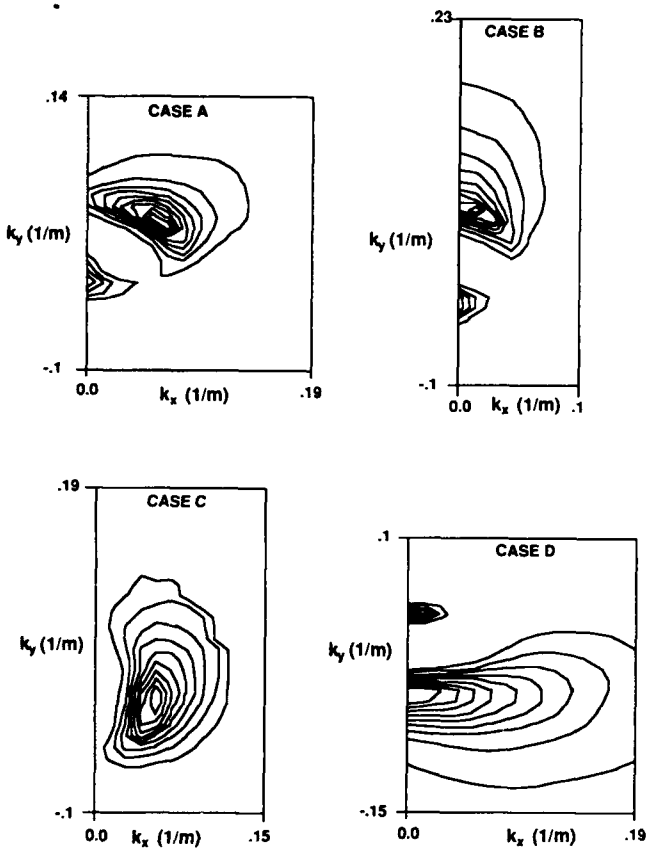

FIG. 6. Normalized contour plots of the 2-D power spectra produced by the DWAVE model.

Table II gives a parametrization of the four surfaces considered. During the course of this 6-h period, the local wind speed decreases as varying amounts of swell from the previous higher winds in the area arrive and contaminate the surface. This and the fact that the forcing conditions were time-varying strongly suggest that the local wind speed will not correlate well with the surface variance. Note that the directions of the sea and swell (ϕ_{sea} and ϕ_{swell}) measured from a fixed but arbitrary coordinate system, as indicated by the spectral peaks, change little from case A to B and then quite dramatically over the next 2 h. The peak wavelength of the swell (Λ_{swell}) shortens considerably during this interval. For case C, Λ_{swell} equals the peak wavelength of sea (Λ_{sea}).

TABLE II. Characteristics of the swell-contaminated surfaces. PM stands for Pierson–Moskowitz.

	Hybrid surfaces				
	A	B	C	D	PM
Time	0:00	2:00	4:00	6:00	···
U (m/s)	12.5	10.0	7.5	5.0	11.0
σ^2_{total} (m^2)	1.21	0.45	0.41	0.44	0.45
σ^2_{swell} (m^2)	0.07	0.03	···	0.01	···
ϕ_{sea} (deg)	30	75	27	270	0
ϕ_{swell} (deg)	270	270	10	90	···
Λ_{sea} (m)	171	119	115	123	83
Λ_{swell} (m)	205	123	115	308	···

The surface variance associated with the swell, σ^2_{swell}, can be estimated simply by integrating over that part of the spectrum that clearly contains the swell. Obviously, for a case such as C, where the bimodal structure is not well resolved, this procedure is not possible. The amount of swell does appear to be generally decreasing in time. It is conceivable that cases A, B, and C show the quieting of a distant source of swell and that case D shows the introduction of a new source of swell. As far as the total surface variance (σ^2_{total}) is concerned, the local seas dominate in all cases. For cases B, C, and D, the sea and swell combine to yield a nearly constant rms surface roughness. It is noted that this roughness is also approximately the same as that of a fully developed sea driven by an 11-m/s wind. Note, however, that the peak wavelengths of these surfaces are much longer than for comparable fully developed seas.

B. Specular scattering

Shown in Fig. 7 are plots of the modeled scattering coefficient, the coherent reflection coefficient, and the coherence in the specular direction for the four cases A, B, C, and D. The scattering geometry is the same as for the previous experiment, i.e., the plane of incidence is the x–z plane and the angle of incidence is 45 deg. Included for comparison purposes are the results for an 11-m/s fully developed sea which, as mentioned earlier, has a surface variance comparable to cases B, C, and D, and a wind speed comparable to local wind during cases A and B.

What is initially striking about these predictions is the variability that can occur over a 2-h time interval. Considering the scattering coefficient, it can be observed that case A shows significantly more loss than the other cases across the frequency range of interest. This is largely due to the fact that case A is much rougher than the other surfaces. The fact that the local wind speed does not characterize the seas very well is again demonstrated quite clearly by the nearly 10-dB

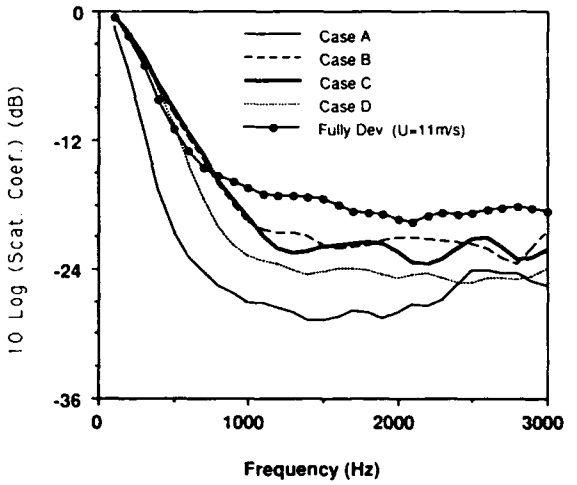

FIG. 7. Comparison of scattering coefficient in the specular direction due to swell-contaminated and fully developed seas.

difference (from 500 Hz up) between the results for the 11-m/s fully developed surface and case A across the frequency band of interest.

Of the swell-contaminated surfaces that have nearly the same total variances (B, C, D), very little difference is observed in the predicted scattering coefficients for frequencies below about 400 Hz. Above this frequency, the scattering coefficient for case D begins to differentiate itself from these other two swell-contaminated surfaces. Cases B and C, on the other hand, continue to track each other quite well across the frequency range shown. Above about 750 Hz, the scattering coefficient predicted for case D is approximately 3 dB lower than for the other two cases. The 11-m/s fully developed case also has a total variance that is nearly equal to these cases (B, C, and D) but its scattering coefficient has a low-frequency rolloff that is faster until about 600 Hz where it abruptly changes slope, and crosses the other predicted scattering coefficients. Above approximately 750 Hz, the fully developed surface has a scattering coefficient that is 3 to 5 dB greater than the closest swell-contaminated surfaces (cases B and C).

C. Nonspecular forward scattering

As we have already seen from sea surfaces that have been generated by uniform, constant generating winds, the forward scattered field nearby but out of the specular direction is influenced by the directional characteristics of the seas. We now consider hybrid surfaces where not only is the local wind not uniform, but the swell and the sea are not usually in the same direction. Case A is a good candidate as a starting point for this analysis since the sea and swell are running in directions fairly perpendicular to each other. Under these conditions, to first order, one would expect that when scattering in the seaward direction ($\phi_s = 225$ deg), variations in the receiver's zenith to be sensitive to waves traveling in the seaward direction while variations in the receiver's azimuth to be sensitive to waves traveling perpendicular to this direction. On the other hand, when scattering into the direction perpendicular to the seaward direction (which for brevity shall be referred to as cross-sea), variations in the receiver's azimuth should be sensitive to waves traveling in the seaward direction while variations in the receiver's zenith be sensitive to waves traveling in the cross-sea direction.

The results of this numerical experiment for a frequency of 300 Hz are shown in Fig. 8. There are several aspects of these comparisons worth noting. First, unlike the fully developed or fetch-limited seas studied earlier, for this swell-contaminated sea Bragg scattering is evident for both scattering orientations, for both azimuthal and zenithal variation. This is obviously due in part to the swell component that happens to have a significant component in a direction perpendicular to the sea direction. Second, from Fig. 9, strong coherence is evident for scattering angles out of the specular direction for the cross-sea orientation as the receiver sweeps in zenith and for the seaward orientation as the receiver sweeps in azimuth. Returning to Fig. 8, these increases in the coherence can be seen to be associated with

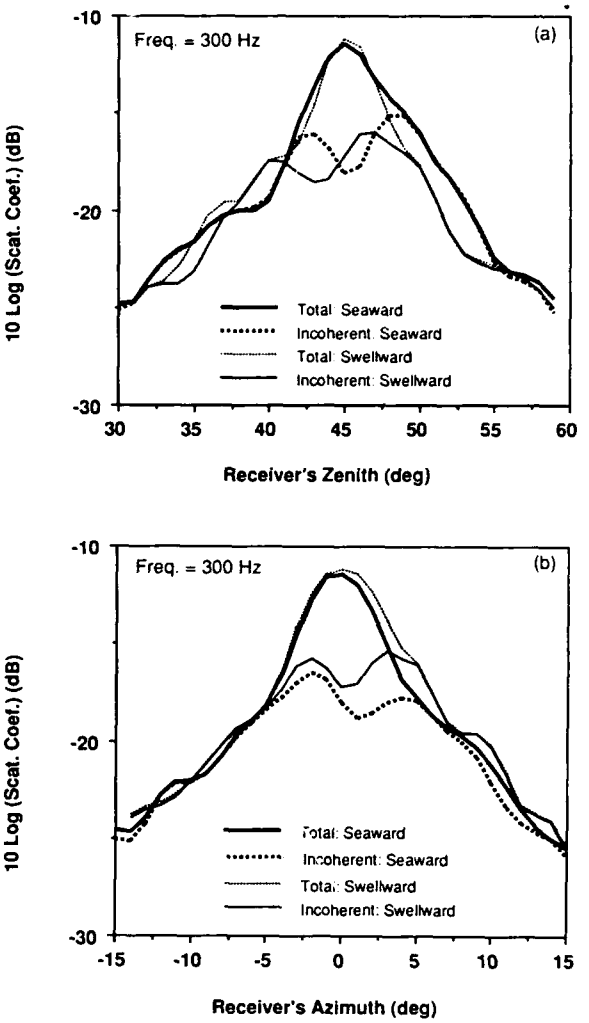

FIG. 8. The effect of surface directionality of case A on the out-of-specular total and incoherent scattering coefficient: (a) zenithal variation, (b) azimuthal variation.

relative decreases in the incoherent component relative to the total scattered energy. It is interesting to note that while significantly less energy is being scattered into these out-of-specular directions (approx. 10 dB down from the specular direction), the energy is quite coherent, a fact that might be significant for experiment in which coherent processing is involved. It should be mentioned, that these sidelobes in the coherence function are not present for fetch-limited or fully developed surfaces containing no swell (calculated but not shown here). In those cases the coherence drops monotonically to less than -30 dB, while for the swell contaminated surface sidelobes that reach -6 dB are achieved. This enhancement in the coherence is not a numerical artifact but a result of the directional character of the sea surface realizations. Unexpected results such as this one confirm the importance of realistically modeling the sea surface in future studies.

In a similar manner, let us now re-examine the surfaces that have nearly the same surface roughness (cases B, C, D, and the fully developed 11-m/s surface). Consider Fig. 10

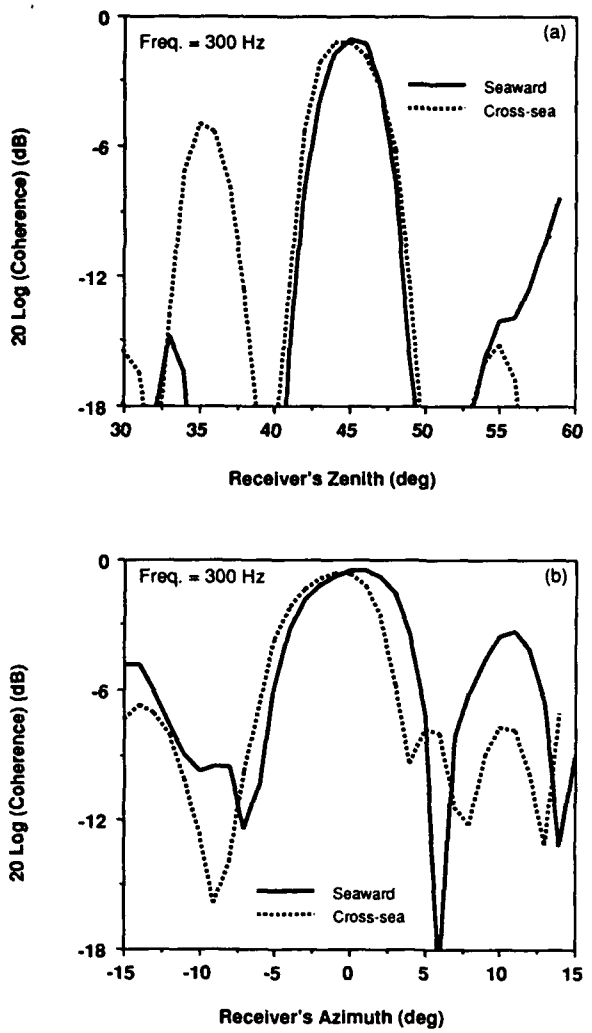

FIG. 9. The effect of surface directionality of case A on the out-of-specular coherence: (a) zenithal variation, (b) azimuthal variation.

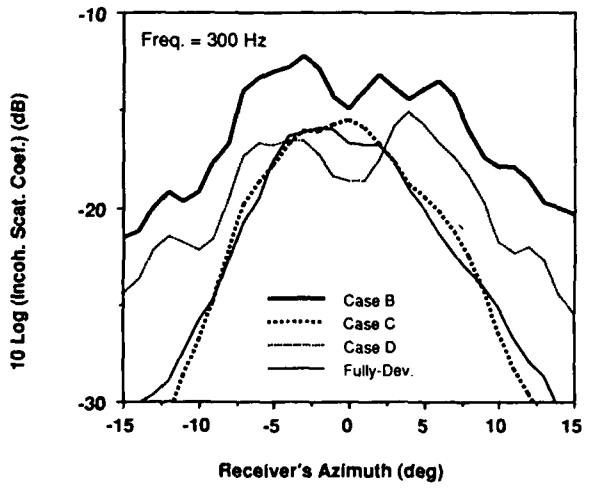

FIG. 10. Comparison of the incoherent scattering coefficient for out-of-specular scattering from swell-contaminated and fully developed surfaces having nearly the same variance.

which shows plots of the incoherent components of the scattering coefficient as a function of the receiver's azimuthal angle at 300 Hz. Again, for this experiment the plane of incidence is the x–y plane and the angle of incidence is 45 deg, which means that by varying the receiver azimuthally, the incoherent component should sense resonances due to surface variations along the y axis. Recalling Fig. 7 one would expect that since cases B and D appear to have similar directional characteristics (i.e., sea and swell traveling along the y axis), their azimuthal dependence should also be similar. On the other hand, case C appears to be directionally very different from these two but not too dissimilar from the spectrum for 11-m/s fully developed case (not shown).

From these figures, it is clear that the acoustic field is sensing the surfaces as expected. Here (and from Fig. 7), we see that cases B and D are oriented with respect to the scattering geometry in a manner that gives rise to a null in the incoherent component that is centered in the specular direction. For these two cases, both components (swell and sea) are traveling almost perpendicular to the plane of incidence; thus a receiver varying in azimuth senses these wavetrains. For case C and the 11-m/s fully developed surface, on the other hand, the waves are traveling in directions nearly parallel to the plane of incidence, so for azimuthal variation of the receiver, the incoherent scattering coefficient is a maximum in the specular direction. Thus we see that the scattering in the forward direction is strongly influenced by the directional characteristics of the surface relative to the scattering geometry. Finally, it is clear from Fig. 10(c) that even though the rms roughnesses for these surfaces are nearly identical, a significant difference in the angular width of the coherence is predicted. Note that case D behaves very much like the fully developed sea that essentially splits the difference between cases B and D.

IV. CONCLUSIONS

The acoustical response to a point source in the forward direction of nonfully developed, directional 2-D sea surfaces have been studied through numerical simulation. Two main regimes were analyzed, namely, fetch-limited seas and swell-contaminated surfaces generated from nonstationary, nonuniform wind fields where waves generated by the local wind and swell generated from distant events combine to produce the local roughness.

For fetch-limited situations (stationary and uniform wind fields), it is concluded that, as expected, in the specular direction, the effect of the fetch reduces essentially to the effect of having a diminished surface roughness. Consequently, the fetch affects the coherence and scattering coefficient for all wind speeds. The shorter the fetch, the higher the frequency at which the coherence begins to degrade. At moderate wind speeds, the scattering coefficient shows deviations up to 10 dB from that estimated for a comparable fully developed surface. In the vicinity of the specular direction, both the fetch and the direction of the wind have a strong effect on the scattered field, especially at low frequencies where discrepancies in excess of 15 dB with respect to the fully developed case have been detected. It is suggested

that this is primarily due to the diminished roughness and the lack of long surface waves in the fetch-limited situation. It is further speculated that whenever the fetch exceeds about half of the crossover fetch for any particular wind speed, differences in the scattering in the specular direction between the fetch-limited and fully developed seas are typically small.

The numerical experiments carried out in this work involving realistic 2-D representations of ocean surfaces generated by nonuniform, nonstationary wind fields show that the scattering coefficient and the coherence of the forward scattered field are strongly influenced by the directional characteristics of the surface and the relative contributions of sea and swell to the roughness. The rapid change of the spectral description of the surface over short periods of time emphasizes the necessity for accurate and timely sea-state descriptions when attempting to model forward scattering. In this regard, the local wind speed or the total rms roughness of the surface are shown to be insufficient descriptors of the sea surface. In particular, it was found that surfaces having the same total roughness and nearly the same local wind speed, but different sea-swell composition, give rise to well-differentiated scattering patterns.

ACKNOWLEDGMENTS

The authors wish to thank George Kerr for making the wave spectra from the DWAVE model available to us and Dr. Don Resio for many useful conversations regarding these spectra and his model (DWAVE). This work has been sponsored by the Office of Naval Research and the Chief of Naval Operations, OP-096. This document (NOARL contribution No. JA 221:024:92) has been reviewed and is approved for public release.

[1] J. W. Caruthers, R. S. Keiffer, and J. C. Novarini, "Near-field acoustic scattering from simulated two-dimensional, wind-driven sea surface," J. Acoust. Soc. Am. **91**, 813–822 (1992).
[2] E. I. Thorsos, "Acoustic scattering from a 'Pierson–Moskowitz' sea surface," J. Acoust. Soc. Am. **88**, 335–349 (1990).
[3] J. W. Caruthers and J. C. Novarini, "Numerical modeling of randomly rough surfaces with application to sea surfaces," Tech. Rep. 71-13-T, Dept. of Oceanography, Texas A&M University (1971).
[4] W. J. Pierson and L. Moskowitz, "A proposed spectral form for fully developed wind seas based on the similarity theory of S. A. Kitaigorodskii," J. Geophys. Res. **69**, 5181–5190 (1964).
[5] K. Hasselman, D. B. Ross, P. Muller, and W. Sell, "A parametric wave prediction model," J. Phys. Oceanogr. **6**, 200–228 (1976).
[6] D. Resio and W. Perrie, "Implications of an f^{-4} equilibrium range for wind-generated waves," J. Phys. Oceanogr. **19**, 193–204 (1989).
[7] B. Kinsman, *Wind Waves* (Prentice-Hall, Englewood Cliffs, NJ, 1965).
[8] L. Fortuin and J. G. Boer, "Spatial and temporal correlation of the sea surface," J. Acoust. Soc. Am. **49**, 1677–1678 (1971).
[9] E. I. Thorsos, "Acoustic scattering from Pierson–Moskowitz seas," J. Acoust. Soc. Am. **88**, 335–349 (1990).
[10] I. Tolstoy and C. S. Clay, *Ocean Acoustics* (McGraw-Hill, New York, 1966).
[11] S. T. McDaniel and D. F. McCammon, "Composite-roughness theory applied to scattering from fetch-limited seas," J. Acoust. Soc. Am. **82**, 1712–1719 (1987).
[12] A. Ishimaru, *Wave Propagation and Scattering in Random Media* (Academic, New York, 1978).